Global cloud-system-resolving simulation of aerosol effect on warm clouds

Kentaroh Suzuki,[1] Teruyuki Nakajima,[2] Masaki Satoh,[2,3] Hirofumi Tomita,[3] Toshihiko Takemura,[4] Takashi Y. Nakajima,[5] and Graeme L. Stephens[1]

Received 23 July 2008; revised 27 August 2008; accepted 5 September 2008; published 10 October 2008.

[1] We simulated the interactions of aerosols with liquid clouds using an aerosol-coupled global cloud-system-resolving model with horizontal resolution of 7 km, and the results are compared with satellite observations of cloud and aerosols. The result shows detailed spatial structures of cloud droplet effective radii (CDR) realistically simulated especially over tropics. The global correlation statistics of liquid water path (LWP) with aerosol index (AI) are investigated for different cloud types to reveal that the LWP slightly decreases with increasing AI, closely resembling satellite-observed features. The CDRs for different cloud types are also shown to decrease with increasing AI, and the sensitivities are found to be relatively similar among cloud types although of discrepancy in absolute values between the model and satellite observation. The model also simulates vertical growth patterns of liquid droplets and their interactions with aerosols in a manner similar to satellite observations. **Citation:** Suzuki, K., T. Nakajima, M. Satoh, H. Tomita, T. Takemura, T. Y. Nakajima, and G. L. Stephens (2008), Global cloud-system-resolving simulation of aerosol effect on warm clouds, *Geophys. Res. Lett.*, *35*, L19817, doi:10.1029/2008GL035449.

1. Introduction

[2] Atmospheric aerosols have been recognized to have a significant effect on cloud microphysical properties referred to as aerosol indirect effect. Current General Circulation Models (GCMs), however, have not yet achieved consistent estimates of the indirect effect [e.g., *Forster et al.*, 2007] despite the increasing efforts of many investigators (see *Lohmann and Feichter* [2005] for review). This is mainly attributed to an inability of GCMs to represent explicit cloud processes due to the much coarser grid size of models than is typical of individual clouds. This is true especially of convective cloud processes represented by cumulus parameterization methods in GCMs although there have recently been several GCM studies of aerosol effects on convective clouds relying on cumulus parameterizations [e.g., *Nober et al.*, 2003; *Menon and Rotstayn*, 2006; *Lohmann*, 2008].

[3] The microphysical processes within the convective clouds are typically governed by air parcels being lifted vertically by buoyant motions. *Rosenfeld* [2000] examined these particle growth processes due to condensation and coalescence in convective clouds using a combined analysis of remotely-sensed cloud droplet effective radius (CDR) near the cloud top and cloud top temperature T_c derived from TRMM measurements. Their results illustrate how the CDR rapidly increases with decreasing T_c (increasing height) for the clouds in clean air masses in contrast to particle growth in polluted conditions. These differences suggest that particle growth is suppressed under polluted conditions which also coincided with an inhibition of rainfall as observed by the TRMM precipitation radar [*Rosenfeld*, 2000]. The difference in the vertical gradient of CDR between pristine and polluted conditions can be conveniently described by the temperature referred to as T_{14} as introduced by *Sekiguchi et al.* [2003]. The T_{14} temperature is defined as the temperature of the T_c-CDR plot where CDR = 14 μm, which is proposed by *Rosenfeld* [2000] as a threshold particle size for initiating drizzle formation. A lower value of T_{14} implies more suppressed growth of CDR than does a higher value of T_{14}. *Sekiguchi et al.* [2003] found a clear negative correlation between observed T_{14} and remotely-sensed aerosol concentrations over global oceans, suggesting a global-scale aerosol suppression of cloud particle growth and thus rain formation.

[4] These aerosol effects on convective clouds need to be represented more explicitly in models than are parameterized in conventional GCMs for advance in our understanding of aerosol-cloud interactions. The global cloud-resolving model NICAM (Nonhydrostatic Icosahedral Atmospheric Model) [e.g., *Satoh et al.*, 2008] recently developed for the Earth Simulator provides a unique tool for this purpose. In this study we implemented an aerosol transport model SPRINTARS (Spectral Radiation-Transport Model for Aerosol Species) [e.g., *Takemura et al.*, 2000] into NICAM. This paper highlights the global characteristics of the aerosol interactions with liquid clouds simulated by NICAM-SPRINTARS.

2. Model Simulation

[5] NICAM has been used for several types of global cloud-resolving experiments with horizontal resolutions of up to 3.5 km [*Satoh et al.*, 2008, and references therein], including a realistic simulation of Madden-Julian Oscillation [*Miura et al.*, 2007]. These studies demonstrate that NICAM reproduces the detailed features of global cloud and precip-

[1]Department of Atmospheric Science, Colorado State University, Fort Collins, Colorado, USA.
[2]Center for Climate System Research, University of Tokyo, Chiba, Japan.
[3]Frontier Research Center for Global Change, Japanese Agency for Marine-Earth Science and Technology, Kanagawa, Japan.
[4]Research Institute for Applied Mechanics, Kyushu University, Fukuoka, Japan.
[5]Department of Network and Computer Engineering, School of Engineering II, Tokai University, Tokyo, Japan.

0094-8276/08/2008GL035449$05.00

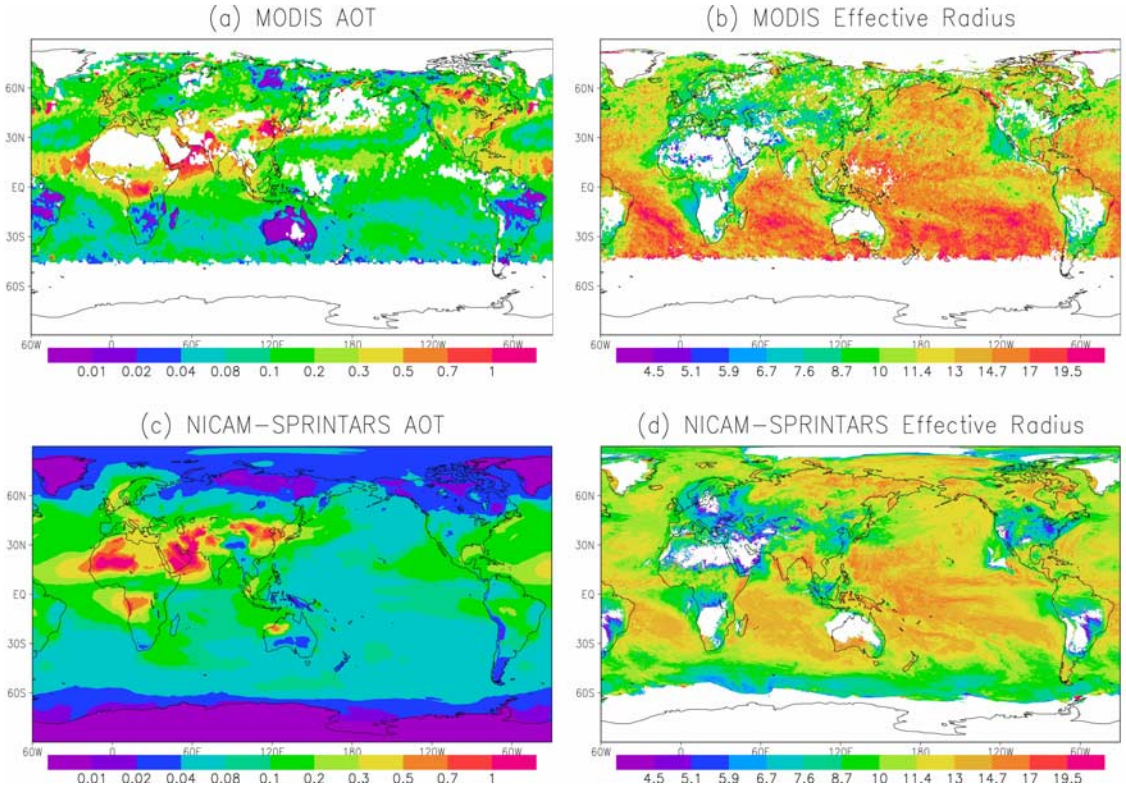

Figure 1. Global distributions of (a and c) AOT and (b and d) CDR in μm obtained from MODIS observations (Figures 1a and 1b) and NICAM-SPRINTARS model (Figures 1c and 1d) for averages during July 1–8, 2006.

itation fields. The implementation of SPRINTARS leads to a representation of aerosol effects on all the resolved liquid clouds including convective clouds as well as stratiform clouds without a cumulus parameterization. A global simulation is performed using NICAM-SPRINTARS with horizontal resolution of 7 km as described in section 1 of the auxiliary material[1]. This resolution with aerosols makes the best use of the state-of-the-art computational resource due to extra needs of machine memory for aerosol tracers.

3. Results

[6] Simulated results using the model are compared with MODerate resolution Imaging Spectroradiometer (MODIS) satellite observations. The procedures of analyses are described in section 2 of the auxiliary material.

3.1. Global Distributions of Aerosol and Cloud

[7] Global distributions of aerosol optical thickness (AOT) and CDR are shown in Figure 1 in comparison with MODIS for AOT at 550 nm [e.g., *Remer et al.*, 2005, 2008] and for CDR retrieved with the algorithm of *Nakajima and Nakajima* [1995] and *Kawamoto et al.* [2001]. Simulated aerosol plumes prevail over the Saharan region as well as over central-southern Africa, Middle East, Europe and East Asia, consistent with MODIS observations (Figures 1a and 1c). Simulated AOTs are, however, smaller than MODIS-retrieved values over North American region, possibly due to insufficient emissions of anthropogenic SO_2 and gas-to-particle production of sulfate aerosols in SPRINTARS. Larger AOTs simulated over Australia are a result of unrealistic dust emissions associated with drier soil moisture. Simulated AOTs are systematically smaller than MODIS values over remote oceans. This is a common bias with traditional GCMs although MODIS also may overestimate AOTs of sea salt due to possible cloud contamination [*Kaufman et al.*, 2005].

[8] A remarkable feature of Figure 1d is the detailed spatial structure of CDR simulated especially over the Tropics. This includes the mixture of large and small particle sizes over central Africa, the north-south contrast over Amazon basin, and the large values zonally found along the ITCZ and the SPCZ. These features have been difficult to simulate with traditional GCMs [e.g., *Suzuki et al.*, 2004]. The model shows, however, larger CDRs than MODIS over Siberia where simulated AOTs are smaller than MODIS values. These differences clearly point to the need for an improved emission inventory and gas-to-particle conversion processes. The simulated CDRs are also smaller than MODIS at mid-to-high latitudes especially over remote oceans. This difference could be reduced by improving rain formation parameterization although satellite retrievals also suffer from various errors [*Kawamoto et al.*, 2001]. It is noteworthy that the MODIS CDRs shown here are retrieved from 3.7 μm radiances [*Nakajima and Nakajima*, 1995] and are systematically smaller than those retrieved from 2.2 μm

[1]Auxiliary materials are available in the HTML. doi:10.1029/2008GL035449.

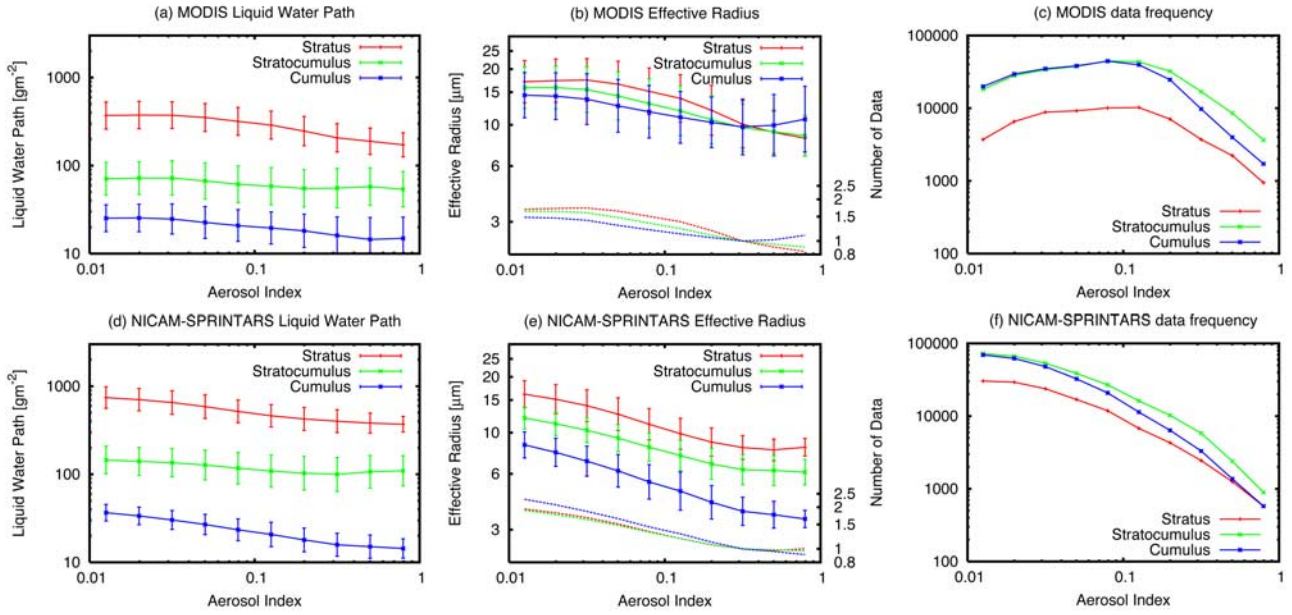

Figure 2. Scatter plot of (a and d) LWP, (b and e) CDR and (c and f) data frequency as a function of AI obtained from MODIS observations (Figures 2a, 2b and 2c) and NICAM-SPRINTARS simulation (Figures 2d, 2e and 2f). Mean values and standard deviation of LWP and CDR are shown as central points and vertical bars, respectively, for each AI bin (Figures 2a, 2b, 2d and 2e). Relative changes of CDR normalized by the value at AI = 0.3 labeled on right axis are also shown by dashed curves in corresponding colors to cloud types (Figures 2b and 2e).

radiances used for NASA standard product [e.g., *Platnick et al.*, 2003]. The 2.2 μm-derived CDRs have been known to be systematically larger than in-situ observations of droplet size distribution [e.g., *Nakajima et al.*, 1991], and the 3.7 μm-derived CDRs lie within two different in-situ measurements [*Platnick and Valero*, 1995]. The difference in CDR between 2.2 μm and 3.7 μm can reflect the in-cloud vertical inhomogeneity [*Nakajima and Nakajima*, 1995]. This issue should be re-visited in comparison with the model that also has an uncertainty in determining the cloud top height as well as relatively coarse resolution and simple microphysical scheme.

3.2. Aerosol-Cloud Correlation Statistics

[9] NICAM-SPRINTARS, incorporating the aerosol effects on resolved explicit cloud processes, provides an opportunity to investigate how the aerosol influences the different types of clouds. We show in Figure 2 correlation statistics of CDR and liquid water path (LWP) derived from CDR and cloud optical thickness as a function of aerosol index (AI) separately for different warm cloud types defined by ISCCP [*Rossow and Schiffer*, 1999]. The data are collected from the whole globe including land and ocean. The AI, defined as the product of AOT and the Ångström Exponent, better represents the column aerosol particle number than does AOT [*Nakajima et al.*, 2001; *Bréon et al.*, 2002], and determining AI < 0.01 from satellite measurement is difficult due to uncertainties for AOT of about 0.015 [*Remer et al.*, 2008]. Figures 2c and 2f illustrate over- and under-estimate in population of light and moderate AI, respectively.

[10] Figures 2a and 2d show encouragingly similar tendencies between the modeled LWP and AI, and the corresponding MODIS values although the modeled LWPs are systematically larger than MODIS, which is common with previous GCM studies [e.g., *Quaas et al.*, 2004]. Both modeled and observed LWPs slightly decrease with AI especially for stratus and cumulus clouds. The correlation between LWP and aerosol amount in previous studies varies in sign and several possible mechanisms were suggested for positive and negative correlations. The aerosol lifetime effect is a candidate for explaining the positive correlations found by *Sekiguchi et al.* [2003] and *Quaas et al.* [2004, 2008] although the positive correlations can also be formed by hygroscopic growth of aerosols [*Storelvmo et al.*, 2006; *Myhre et al.*, 2007]. In contrast to these studies, *Matsui et al.* [2006] observationally reported a decreasing trend of LWP with increasing AI similar to that of Figure 2. A possible explanation for the negative correlation can be provided by semi-direct effect [*Hansen et al.*, 1997] as well as by rain wash-out effect [*Suzuki et al.*, 2004]. The correlation patterns can actually be interpreted as formed by a non-linear global balance between these positive and negative tendencies associated with above mechanisms [*Suzuki et al.*, 2004]. The small negative correlations found in Figures 2a and 2d suggest that the negative tendencies slightly predominate the positive tendencies with different extents depending on cloud types. It should be noted that the correlation statistics may vary with how to sample the data [e.g., *Sekiguchi et al.*, 2003; *Matsui et al.*, 2006], and more regional analysis is also important in future studies.

[11] Figures 2b and 2e show similar negative correlations of CDR with AI as expected from the first indirect effect. The optically thinner types of clouds (stratocumulus and cumulus) are, however, found to have smaller CDRs than observed by MODIS. Relative changes of CDR with AI are

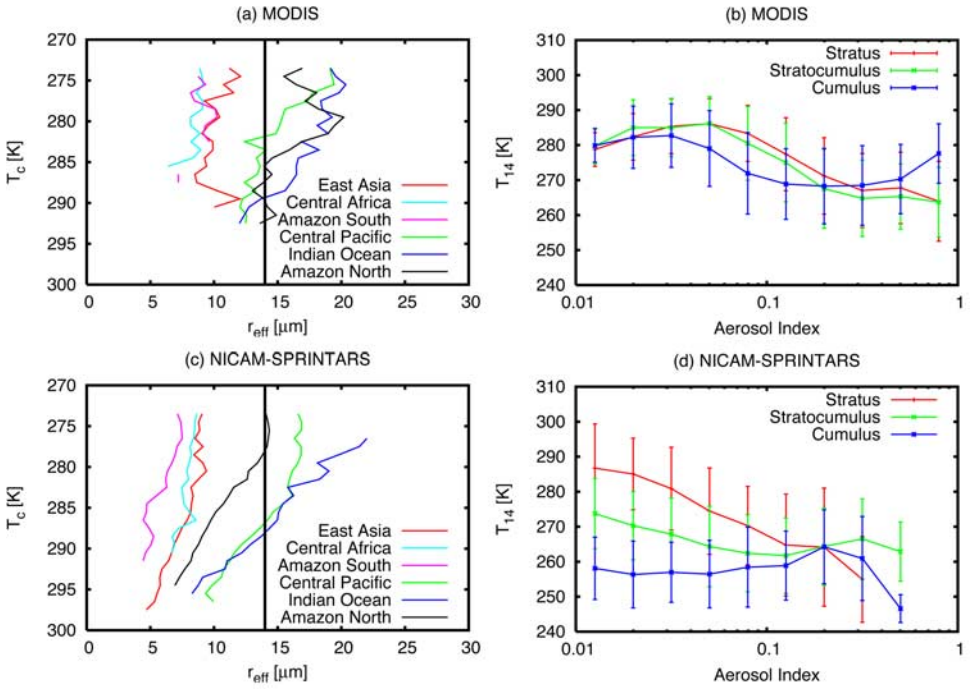

Figure 3. (a and c) T_c-CDR plots for several places across the globe obtained from MODIS (Figure 3a) and NICAM-SPRINTARS (Figure 3c). Mean values of CDR are shown in corresponding colors to region for each 1 K bin of T_c along with $r_e = 14$ μm shown as vertical lines. (b and d) Scatter plot of T_{14} as a function of AI (see text for details) obtained from MODIS (Figure 3b) and NICAM-SPRINTARS (Figure 3d). Mean values and standard deviations of T_{14} are shown as central points and vertical bars, respectively, for each AI bin.

more similar between the model and MODIS with a sensitivity of $d \ln r_e / d \ln AI \approx -0.176$ that is relatively common among cloud types although of slightly different sensitivities especially between cumulus and stratus clouds. This tendency is represented oppositely by the model and MODIS analysis although not clear due to large variability of CDR indicated by long vertical bars.

3.3. Vertical Growth Pattern of Cloud Particle

[12] NICAM-SPRINTARS resolves convective motions of cloud and aerosol particles and then provides the first opportunity to use model data to analyze vertical growth processes of cloud particles and their interactions with aerosols on global scale. We present in Figures 3a and 3c these model results in the form of T_c-CDR suggested by *Rosenfeld* [2000] for comparison with MODIS observations. Figures 3a and 3c illustrate that the clouds chosen from clean regions, i.e., central Pacific Ocean, Indian Ocean and Northern Amazon, exhibit a rapid growth of CDR to reach 14 μm in both MODIS and the model although of different slopes implying different representations of particle growth rate. The clouds over polluted regions such as East Asia, central Africa and Southern Amazon demonstrate more suppressed particle growth. These features resemble those obtained from previous observations by *Rosenfeld* [2000].

[13] Figure 3b shows the comparison for global correlations of T_{14} with AI separately for different ISCCP cloud types. Negative correlations of T_{14} with AI > 0.03–0.04 found in MODIS especially for stratus and stratocumulus clouds suggest a global-scale suppression of liquid particle growth by aerosols, consistent with a previous observational study [*Sekiguchi et al.*, 2003]. The T_{14} of cumulus clouds show systematically lower values and are more independent of AI. Figure 3d shows that the model reproduces the negative correlations of T_{14} with AI for stratus and stratocumulus clouds although stratocumulus shows lower T_{14} values than MODIS, reflecting the smaller simulated CDRs than MODIS for stratocumulus. The simulated T_{14} for cumulus clouds tends to be independent of AI consistently with MODIS although of smaller absolute values due to smaller CDRs.

4. Conclusion

[14] This paper highlights the simulated results of aerosol interactions with liquid clouds using a global cloud-system-resolving model coupled with an aerosol transport model based on horizontal resolution of 7 km. The model, for the first time, resolves the vertical growth of cloud particles due to convective air motions coupled with aerosols on global scale. It is demonstrated that the model simulates T_c-CDR plot as well as detailed spatial structure of CDR and correlation statistics of CDR and LWP with aerosols for different cloud types. NICAM-SPRINTARS will further be used in future studies for more detailed investigations of the aerosol-cloud interactions reported here, including additional studies of deep-convective clouds with aerosol effects on ice-phase processes.

[15] **Acknowledgments.** We are grateful to N. Schutgens and T. Mitsui for helping run the model, and to two reviewers and S. van den

Heever for their valuable comments. This research was supported by the Global Environment Research Fund B-4 of the Ministry of Environment, RR2002 and the Data Integration for Earth Observation projects of MEXT, JAXA/ADEOS-II GLI project, JST/CREST, NASA grant NNX07AR11G and the NOAA grant under the NOAA cooperative agreement NA17RJ1228. MODIS aerosol product was provided by NASA/GSFC.

References

Bréon, F.-M., D. Tanre, and S. Generoso (2002), Aerosol effect on cloud droplet size monitored from satellite, *Science*, *295*, 834–838.

Forster, P., et al. (2007), Changes in atmospheric constituents and in radiative forcing, in *Climate Change 2007: The Physical Science Basis. Contribution of Working Group I to the Fourth Assessment Report of the Intergovernmental Panel on Climate Change*, edited by S. Solomon et al., pp. 129–234, Cambridge Univ. Press, Cambridge, U. K.

Hansen, J., M. Sato, and R. Rueby (1997), Radiative forcing and climate response, *J. Geophys. Res.*, *102*, 6831–6864.

Kaufman, Y. J., O. Boucher, D. Tanre, M. Chin, L. A. Remer, and T. Takemura (2005), Aerosol anthropogenic component estimated from satellite data, *Geophys. Res. Lett.*, *32*, L17804, doi:10.1029/2005GL023125.

Kawamoto, K., T. Nakajima, and T. Y. Nakajima (2001), A global determination of cloud microphysics with AVHRR remote sensing, *J. Clim.*, *14*, 2054–2068.

Lohmann, U. (2008), Global anthropogenic aerosol effects on convective clouds in ECHAM5-HAM, *Atmos. Chem. Phys.*, *8*, 2115–2131.

Lohmann, U., and J. Feichter (2005), Global indirect aerosol effects: A review, *Atmos. Chem. Phys.*, *5*, 715–737.

Matsui, T., H. Masunaga, S. M. Kreidenweis, R. A. Pielke Sr., W.-K. Tao, M. Chin, and Y. J. Kaufman (2006), Satellite-based assessment of marine low cloud variability associated with aerosol, atmospheric stability, and the diurnal cycle, *J. Geophys. Res.*, *111*, D17204, doi:10.1029/2005JD006097.

Menon, S., and L. Rotstayn (2006), The radiative influence of aerosol effects on liquid-phase cumulus and stratiform clouds based on sensitivity studies with two climate models, *Clim. Dyn.*, *27*, 345–356.

Miura, H., et al. (2007), A Madden-Julian Oscillation event realistically simulated by a global cloud-resolving model, *Science*, *318*, 1763–1765.

Myhre, G., et al. (2007), Aerosol-cloud interaction inferred from MODIS satellite data and global aerosol models, *Atmos. Chem. Phys.*, *7*, 3081–3101.

Nakajima, T. Y., and T. Nakajima (1995), Wide-area determination of cloud microphysical properties from NOAA AVHRR measurements for FIRE and ASTEX regions, *J. Atmos. Sci.*, *52*, 4043–4059.

Nakajima, T., et al. (1991), Determination of the optical thickness and effective particle radius of clouds from reflected solar radiation measurements. Part II: Marine stratocumulus observations, *J. Atmos. Sci.*, *48*, 728–750.

Nakajima, T., A. Higurashi, K. Kawamoto, and J. E. Penner (2001), A possible correlation between satellite-derived cloud and aerosol microphysical parameters, *Geophys. Res. Lett.*, *28*, 1171–1174.

Nober, F. J., H.-F. Graf, and D. Rosenfeld (2003), Sensitivity of the global circulation to the suppression of precipitation by anthropogenic aerosols, *Global Planet. Change*, *37*, 57–80.

Platnick, S., and F. P. J. Valero (1995), A validation of a satellite cloud retrieval during ASTEX, *J. Atmos. Sci.*, *52*, 2985–3001.

Platnick, S., et al. (2003), The MODIS cloud products: Algorithms and examples from Terra, *IEEE Trans. Geosci. Remote Sens.*, *41*, 459–473.

Quaas, J., O. Boucher, and F.-M. Bréon (2004), Aerosol indirect effects in POLDER satellite data and the Laboratoire de Météorologie Dynamique-Zoom (LMDZ) general circulation model, *J. Geophys. Res.*, *109*, D08205, doi:10.1029/2003JD004317.

Quaas, J., O. Boucher, N. Bellouin, and S. Kinne (2008), Satellite-based estimate of the direct and indirect aerosol climate forcing, *J. Geophys. Res.*, *113*, D05204, doi:10.1029/2007JD008962.

Remer, L. A., et al. (2005), The MODIS aerosol algorithm, products, and validation, *J. Atmos. Sci.*, *62*, 947–973.

Remer, L. A., et al. (2008), Global aerosol climatology from the MODIS satellite sensors, *J. Geophys. Res.*, *113*, D14S07, doi:10.1029/2007JD009661.

Rosenfeld, D. (2000), Suppression of rain and snow by urban and industrial air pollution, *Science*, *287*, 1793–1796.

Rossow, W. B., and R. A. Schiffer (1999), Advances in understanding clouds from ISCCP, *Bull. Am. Meteorol. Soc.*, *80*, 2261–2287.

Satoh, M., et al. (2008), Nonhydrostatic Icosahedral Atmospheric Model (NICAM) for global cloud resolving simulations, *J. Comput. Phys.*, *227*, 3486–3514.

Sekiguchi, M., T. Nakajima, K. Suzuki, K. Kawamoto, A. Higurashi, D. Rosenfeld, I. Sano, and S. Mukai (2003), A study of the direct and indirect effects of aerosols using global satellite data sets of aerosol and cloud parameters, *J. Geophys. Res.*, *108*(D22), 4699, doi:10.1029/2002JD003359.

Storelvmo, T., et al. (2006), Combined observational and modeling based study of the aerosol indirect effect, *Atmos. Chem. Phys.*, *6*, 3585–3601.

Suzuki, K., et al. (2004), A study of the aerosol effect on a cloud field with simultaneous use of GCM modeling and satellite observation, *J. Atmos. Sci.*, *61*, 179–194.

Takemura, T., H. Okamoto, Y. Maruyama, A. Numaguti, A. Higurashi, and T. Nakajima (2000), Global three-dimensional simulation of aerosol optical thickness distribution of various origins, *J. Geophys. Res.*, *105*, 17,853–17,873.

T. Nakajima and M. Satoh, Center for Climate System Research, University of Tokyo, Kashiwa, Chiba 277-8568, Japan.

T. Y. Nakajima, Department of Network and Computer Engineering, School of Engineering II, Tokai University, Shibuya, Tokyo 151-0063, Japan.

G. L. Stephens and K. Suzuki, Department of Atmospheric Science, Colorado State University, Fort Collins, CO 80523-1371, USA. (kenta@atmos.colostate.edu)

T. Takemura, Research Institute for Applied Mechanics, Kyushu University, Kasuga, Fukuoka 816-8580, Japan.

H. Tomita, Frontier Research Center for Global Change, Japanese Agency for Marine-Earth Science and Technology, Yokohama-city, Kanagawa 236-0001, Japan.